Pergamon PII: S0038–092X(99)00055–9
www.elsevier.com/locate/solener
Solar Energy Vol. 68, No. 1, pp. 33–48, 2000

0038-092X/00/$ - see front matter

ON THE CLEAR SKY MODEL OF THE ESRA — EUROPEAN SOLAR RADIATION ATLAS — WITH RESPECT TO THE HELIOSAT METHOD

CHRISTELLE RIGOLLIER†, OLIVIER BAUER and LUCIEN WALD
Groupe Télédétection et Modélisation, Ecole des Mines de Paris, BP 207, 06904 Sophia Antipolis cedex, France

Received 25 January 1999; revised version accepted 4 June 1999

Communicated by RICHARD PEREZ

Abstract—This paper presents a clear-sky model, which has been developed in the framework of the new digital European Solar Radiation Atlas (ESRA). This ESRA model is described and analysed with the main objective of being used to estimate solar radiation at ground level from satellite images with the Heliosat method. Therefore it is compared to clear-sky models that have already been used in the Heliosat method. The diffuse clear-sky irradiation estimated by this ESRA model and by other models has been also checked against ground measurements, for different ranges of the Linke turbidity factor and solar elevation. The results show that the ESRA model is the best one with respect to robustness and accuracy. The r.m.s. error in the estimation of the hourly diffuse irradiation ranges from 11 Wh m^{-2} to 35 Wh m^{-2} for diffuse irradiation up to 250 Wh m^{-2}. The good results obtained with such a model are due to the fact that it takes into account the Linke turbidity factor and the elevation of the site, two factors that influence the incoming solar radiation. In return, it implies the knowledge of these factors at each pixel of the satellite image for the application of the Heliosat method.

1. INTRODUCTION

In the course of the realisation of the first edition of the new digital European Solar Radiation Atlas for years 1981–1990 (Wald *et al*., 1999; ESRA), new models have been devised for the computation of the irradiance and further of the irradiation for clear skies by Page (1995). Compared to the model used for the European Solar Radiation Atlas for years 1966–1975 (Palz, 1984), there is an explicit expression for both the beam and the diffuse components. The parameters of these models have been empirically adjusted by fitting techniques using hourly measurements spanned over several years and for several locations in Europe. The Linke turbidity factor is a key point in these models. It is a function of the scattering by aerosols and the absorption by gas, mainly water vapour. When combined with the atmosphere molecule scattering, it summarises the turbidity of the atmosphere, and hence the attenuation of the direct beam and the importance of the diffuse fraction. The larger the Linke turbidity factor, the larger the attenuation of the radiation by the clear-sky atmosphere. Clear-sky models are instrumental in several applications in solar energy. Of particular interest to the authors is the assessment of the solar radiation from satellite images. In the Heliosat method, one of the most known methods, the clear-sky model is a central point. Cano *et al*. (1986) used the model of Bourges (1979), Moussu *et al*. (1989) a very similar one but from Perrin de Brichambaut and Vauge (1982). The clear-sky model (Kasten model) of the 1966–1975 Atlas (Palz, 1984) has been recently introduced in the Heliosat method by the team of the University of Oldenburg (Heinemann, personal communication). The better the clear-sky model, the better the assessment of the irradiation from satellite observations. For that reason, the authors investigated the new models proposed by the ESRA.

The present article details and comments on these models, including several graphs, therefore providing a more comprehensive description of these models useful for discussing its relevance to the Heliosat method. It also discusses the differences between the concurrent models proposed by the ESRA and concludes on their relevance for the computation of either the irradiance or the irradiation. Symbols used in this paper are those recommended by the ESRA.

†Author to whom correspondence should be addressed. Tel.: +33-4-9395-7449; fax: +33-4-9395-7535; e-mail: christelle.rigollier@cenerg.cma.fr

2. THE HORIZONTAL GLOBAL IRRADIANCE UNDER CLOUDLESS SKIES

2.1. The beam component

In this model, the global horizontal irradiance for clear sky, G_c, is split into two parts: the direct component, B_c, and the diffuse component, D_c. Each component is determined separately. The unit for irradiance is W m^{-2}. The direct irradiance on a horizontal surface (or beam horizontal irradiance) for clear sky, B_c, is given by:

$$B_c = I_0 \varepsilon \sin \gamma_s \exp(-0.8662 T_L(\mathrm{AM2})\, m \delta_R(m)) \tag{1}$$

where I_0 is the solar constant, that is the extraterrestrial irradiance normal to the solar beam at the mean solar distance. It is equal to 1367 W m^{-2}; ε is the correction used to allow for the variation of sun–earth distance from its mean value; γ_s is the solar altitude angle. γ_s is 0° at sunrise and sunset; $T_L(\mathrm{AM2})$ is the Linke turbidity factor for an air mass equal to 2; m is the relative optical air mass; $\delta_R(m)$ is the integral Rayleigh optical thickness.

The quantity:

$$\exp(-0.8662 T_L(\mathrm{AM2})\, m \delta_R(m)) \tag{2}$$

represents the beam transmittance of the beam radiation under cloudless skies. The relative optical air mass m expresses the ratio of the optical path length of the solar beam through the atmosphere to the optical path through a standard atmosphere at sea level with the sun at the zenith. As the solar altitude decreases, the relative optical path length increases. The relative optical path length also decreases with increasing station height above the sea level, z. A correction procedure is applied, obtained as the ratio of mean atmospheric pressure, p, at the site elevation, to mean atmospheric pressure at sea level, p_0. This correction is particularly important in mountainous areas. The relative optical air mass has no unit; it is given by Kasten and Young (1989), where γ_s^{true} is in degrees:

$$m(\gamma_s^{\mathrm{true}}) = \frac{(p/p_0)}{\sin \gamma_s^{\mathrm{true}} + 0.50572\,(\gamma_s^{\mathrm{true}} + 6.07995)^{-1.6364}} \tag{3}$$

with the station height correction given by:

$$p/p_0 = \exp(-z/z_h) \tag{4}$$

where z is the site elevation and z_h is the scale height of the Rayleigh atmosphere near the Earth surface, equal to 8434.5 m.

The solar altitude angle used in Eq. (3), γ_s^{true}, is corrected for refraction:

$$\gamma_s^{\mathrm{true}} = \gamma_s + \Delta\gamma_{\mathrm{refr}} \tag{5}$$

$$\Delta\gamma_{\mathrm{refr}} = 0.061359(180/\pi) \times \frac{0.1594 + 1.1230(\pi/180)\gamma_s + 0.065656(\pi/180)^2\gamma_s^2}{1 + 28.9344(\pi/180)\gamma_s + 277.3971(\pi/180)^2\gamma_s^2} \tag{6}$$

The Rayleigh optical thickness, δ_R, is the optical thickness of a pure Rayleigh scattering atmosphere, per unit of air mass, along a specified path length. As the solar radiation is not monochromatic, the Rayleigh optical thickness depends on the precise optical path and hence on relative optical air mass, m. The parametrisation used is the following (Kasten, 1996):

$$\begin{cases} \text{if } m \le 20 \quad (\gamma_s \ge 1.9°), \\ 1/\delta_R(m) = 6.62960 + 1.75130m \\ \quad - 0.12020m^2 + 0.00650m^3 - 0.00013m^4 \\ \text{if } m > 20 \quad (\gamma_s < 1.9°), \\ 1/\delta_R(m) = 10.4 + 0.718m \end{cases} \tag{7}$$

The discrepancy between both formulae at $m = 20$ is equal to 1.6×10^{-2}, which is negligible (less than 0.1% of $1/\delta_R(m)$).

All the variation of the beam transmittance with air mass is included in the product $m\delta_R(m)$. Fig. 1 displays the beam transmittance (a) and irradiance (b) for $p = p_0$ (sea level), and for different values of turbidity factor ($T_L(\mathrm{AM2}) = 2, 3, 5, 7$), as a function of solar elevation.

2.2. The diffuse component

The diffuse irradiance falling on a horizontal surface for clear sky (or diffuse horizontal irradiance), D_c, also depends on the Linke turbidity factor, $T_L(\mathrm{AM2})$, at any solar elevation. In fact, the proportion of the scattered energy in the atmosphere increases as the turbidity increases, and as the beam irradiance falls, the diffuse irradiance normally rises. At very low solar altitudes and high turbidity, however, the diffuse irradiance may fall with turbidity increase due to high overall radiative energy loss in the atmosphere associated with long path length. Thus, the diffuse horizontal irradiance, D_c, is determined by:

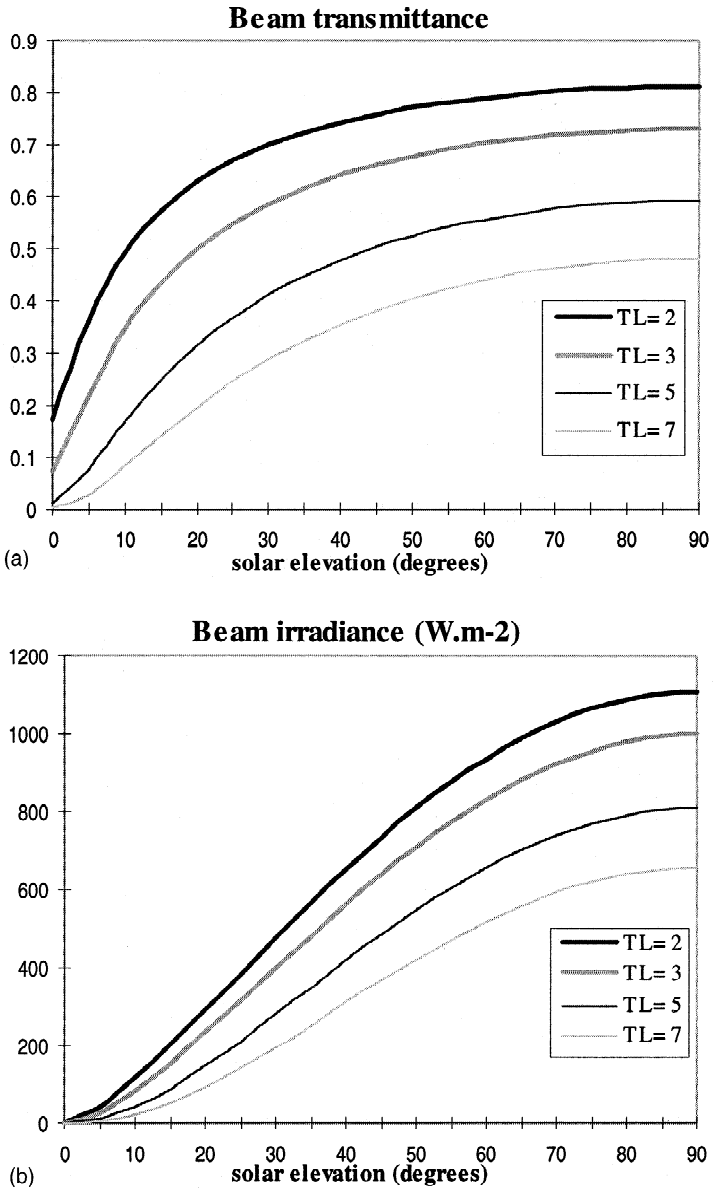

Fig. 1. (a) The beam transmittance. (b) The beam horizontal irradiance for clear sky, B_c.

$$D_c = I_0 \varepsilon T_{rd}(T_L(\mathrm{AM2}))F_d(\gamma_s, T_L(\mathrm{AM2})) \quad (8)$$

In this equation, the diffuse radiation is expressed as the product of the diffuse transmission function at zenith (i.e. sun elevation is 90°), T_{rd}, and a diffuse angular function, F_d.

$$T_{rd}(T_L(\mathrm{AM2})) = -1.5843 \times 10^{-2} + 3.0543 \times 10^{-2} T_L(\mathrm{AM2}) + 3.797 \times 10^{-4}[T_L(\mathrm{AM2})]^2 \quad (9)$$

For very clear sky, the diffuse transmission function is very low: there is almost no diffusion, but by the air molecules. As the turbidity increases, the diffuse transmittance increases while the direct transmittance decreases. Typically, T_{rd} ranges from 0.05 for very clear sky ($T_L(\mathrm{AM2}) = 2$) to 0.22 for very turbid atmosphere ($T_L(\mathrm{AM2}) = 7$). Fig. 2 displays T_{rd} as a function of $T_L(\mathrm{AM2})$.

The diffuse angular function, F_d, depends on the solar elevation angle and is fitted with the help of second order sine polynomial functions:

$$F_d(\gamma_s, T_L(\mathrm{AM2})) = A_0 + A_1 \sin(\gamma_s) + A_2[\sin(\gamma_s)]^2 \quad (10)$$

The coefficients A_0, A_1, and A_2, only depend on the Linke turbidity factor. They are unitless and are given by:

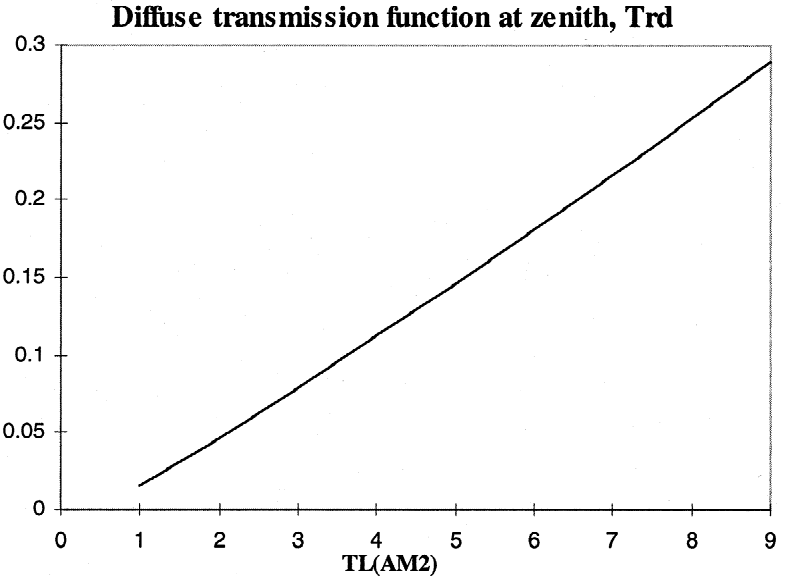

Fig. 2. The diffuse transmission function at zenith, T_{rd}, as a function of the Linke turbidity factor $T_L(AM2)$.

$$\begin{cases} A_0 = 2.6463 \times 10^{-1} - 6.1581 \times 10^{-2} T_L(AM2) + 3.1408 \times 10^{-3} [T_L(AM2)]^2 \\ A_1 = 2.0402 + 1.8945 \times 10^{-2} T_L(AM2) - 1.1161 \times 10^{-2} [T_L(AM2)]^2 \\ A_2 = -1.3025 + 3.9231 \times 10^{-2} T_L(AM2) + 8.5079 \times 10^{-3} [T_L(AM2)]^2 \end{cases} \quad (11)$$

with a condition on A_0:

$$\text{if } (A_0.T_{rd}) < 2 \times 10^{-3}, A_0 = 2 \times 10^{-3} / T_{rd}. \quad (12)$$

This condition is required because A_0 yielded negative values for $T_L(AM2) > 6$. It was therefore decided to impose this limiting condition to achieve acceptable values at sunrise and sunset.

The diffuse function is represented in Fig. 3. One can note that F_d is not exactly equal to 1 for $\gamma_s = 90°$. Eq. (8) suggests that this should be the case, whatever the turbidity. The model can be improved on that point.

Once F_d is computed, the diffuse horizontal irradiance, D_c can be determined. It is displayed in Fig. 4 for several Linke turbidity factors, as a function of the solar elevation. D_c clearly increases as the turbidity increases, due to the

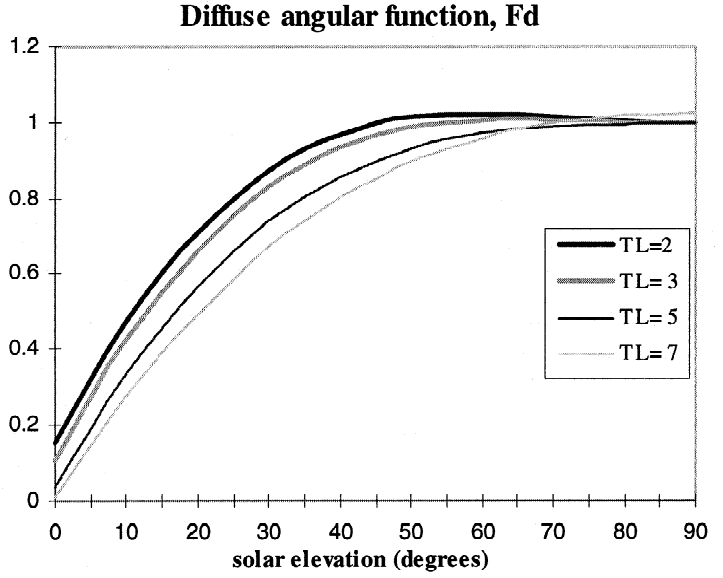

Fig. 3. The diffuse solar zenith function, F_d.

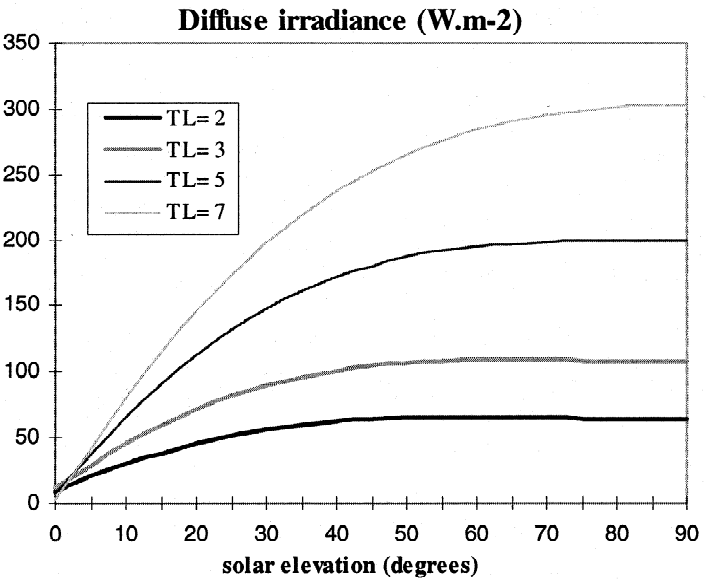

Fig. 4. The diffuse horizontal irradiance for clear sky, D_c.

increase in scattering by the aerosols. As already mentioned, it may be the opposite at very low solar altitudes and high turbidity.

Then, the direct and diffuse irradiances under cloudless sky conditions can be summed to yield the global clear sky horizontal irradiance, which is represented in Fig. 5:

$$G_c = B_c + D_c. \tag{13}$$

The global irradiance decreases as the turbidity increases and as the solar elevation decreases. It is not equal to 0 at sunset or sunrise because of the diffuse component which is still noticeable while the sun is below the horizon.

3. THE HORIZONTAL GLOBAL IRRADIATION UNDER CLOUDLESS SKIES

3.1. The beam component

Once m, T_L(AM2), and $\delta_R(m)$ are known, the cloudless beam horizontal irradiation can be evaluated for any part of the day by numerical integration of B_c using suitable time steps. The site, however, may be partially obstructed and/or

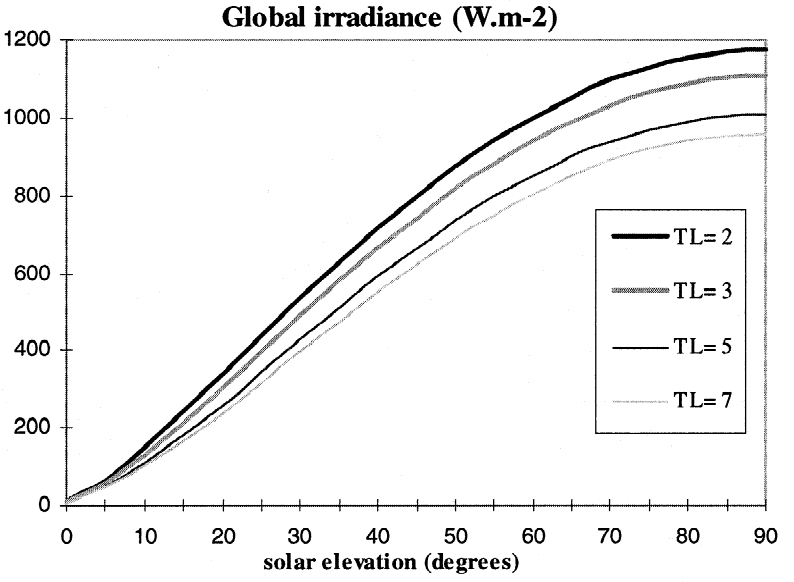

Fig. 5. The global horizontal irradiance for clear sky, G_c.

the beam may not shine on a certain surface of interest for part of the time period inspected. Using a range of techniques, like shading masks on solar charts, it is possible to identify the periods of day during which the beam will actually reach the surface. The numerical integration can be adjusted for this, but the task becomes easier if the solutions can be assessed analytically rather than numerically. Thus the beam irradiance has been constructed by data fitting techniques to provide a T_L(AM2)-dependent output that can be handled with ease analytically. It takes the form:

$$B_c = I_0 \varepsilon T_{rb}(T_L(\mathrm{AM2}))F_b(\gamma_s, T_L(\mathrm{AM2})) \quad (14)$$

where $T_{rb}(T_L(\mathrm{AM2}))$ is a transmission function for beam radiation at zenith and F_b is a beam angular function. B_c is set to 0 if Eq. (14) leads to a negative value. The computation of T_{rb} is made at zenith, i.e. sun elevation is 90°. So, in this case the relative optical air mass m is given by p/p_0. Thus, T_{rb} is only dependent on the Linke turbidity factor for air mass 2 and on p/p_0 which is determined by the site elevation:

$$T_{rb}(T_L(\mathrm{AM2})) = \exp\left[-0.8662\, T_L(\mathrm{AM2})\left(\frac{p}{p_0}\right)\delta_R\left(\frac{p}{p_0}\right)\right] \quad (15)$$

$F_b(\gamma_s, T_L(\mathrm{AM2}))$ has the form of a second order polynomial on the sine of the solar altitude, γ_s, with coefficients solely dependent on T_L(AM2):

$$F_b(\gamma_s, T_L(\mathrm{AM2})) = C_0 + C_1 \sin(\gamma_s) + C_2[\sin(\gamma_s)]^2 \quad (16)$$

Eq. (14) corresponds to a re-writing of the beam irradiance, using the form used for the diffuse irradiance (Eq. (8)).

Setting $F_b(\gamma_s, T_L(\mathrm{AM2}))$ to 0 or very close to 0 may produce negative values at high turbidities. This situation which arises only at very low altitudes results because the polynomials are not a perfect fit. To increase the accuracy of the fits at very low solar elevation, the values of the coefficients C_0, C_1 and C_2 were computed for three ranges of the solar altitude angle at noon, γ_s^{noon}: below 15°, between 15° and 30°, and over 30°. Thus the polynomials take the form:

$$\begin{cases} C_0 = L_{00} + L_{01}T_L(\mathrm{AM2})(p/p_0) + L_{02}[T_L(\mathrm{AM2})(p/p_0)]^2 \\ C_1 = L_{10} + L_{11}T_L(\mathrm{AM2})(p/p_0) + L_{12}[T_L(\mathrm{AM2})(p/p_0)]^2 \\ C_2 = L_{20} + L_{21}T_L(\mathrm{AM2})(p/p_0) + L_{22}[T_L(\mathrm{AM2})(p/p_0)]^2 + L_{23}[T_L(\mathrm{AM2})(p/p_0)]^3 \end{cases} \quad (17)$$

with the L_{ij} coefficients listed in Table 1 for the three considered ranges. These coefficients, as well as C_i, B_i, and D_i (see further) are unitless.

Finally, the analytical integral of the beam irradiation for a period ranging from solar hour angles ω_1 to ω_2, takes the form:

$$B_c(\omega_1, \omega_2) = I_0 \varepsilon T_{rb}(T_L(\mathrm{AM2}))\int_{\omega_1}^{\omega_2} F_b(\gamma_s, T_L(\mathrm{AM2}))\left(\frac{Dl}{2\pi}\right)\mathrm{d}\omega \quad (18)$$

where Dl is the length of the day, i.e. 24 h or 86,400 s, and ω_1 to ω_2 are solar angles related to two instants t_1 and t_2 (expressed in decimal hour), according to the following equations:

$$\begin{aligned} \omega_1 &= (t_1 - 12)\pi/12 \\ \omega_2 &= (t_2 - 12)\pi/12 \end{aligned} \quad (19)$$

The solar hour angle, ω, expresses the time of the day in terms of the angle of rotation of the Earth about its axis from its solar noon position at a specific place. As the Earth rotates 360° (or 2π rad) in 24 h, in 1 h the rotation is 15° (or $\pi/12$ rad).

The unit of $B_c(\omega_1, \omega_2)$ is Wh m^{-2} if the length

Table 1. Coefficients L_{ij} for the computation of the C_i coefficients

C_0	L_{00}	L_{01}	L_{02}	
$\gamma_s^{noon} > 30°$	-1.7349×10^{-2}	-5.8985×10^{-3}	6.8868×10^{-4}	
$15° < \gamma_s^{noon} \le 30°$	-8.2193×10^{-3}	4.5643×10^{-4}	6.7916×10^{-5}	
$\gamma_s^{noon} \le 15°$	-1.1656×10^{-3}	1.8408×10^{-4}	-4.8754×10^{-7}	
C_1	L_{10}	L_{11}	L_{12}	
$\gamma_s^{noon} > 30°$	1.0258	-1.2196×10^{-1}	1.9229×10^{-3}	
$15° < \gamma_s^{noon} \le 30°$	8.9233×10^{-1}	-1.9991×10^{-1}	9.9741×10^{-3}	
$\gamma_s^{noon} \le 15°$	7.4095×10^{-1}	-2.2427×10^{-1}	1.5314×10^{-2}	
C_2	L_{20}	L_{21}	L_{22}	L_{23}
$\gamma_s^{noon} > 30°$	-7.2178×10^{-3}	1.3086×10^{-1}	-2.8405×10^{-3}	0
$15° < \gamma_s^{noon} \le 30°$	2.5428×10^{-1}	2.6140×10^{-1}	-1.7020×10^{-2}	0
$\gamma_s^{noon} \le 15°$	3.4959×10^{-1}	7.2313×10^{-1}	-1.2305×10^{-1}	5.9194×10^{-3}

of the day is expressed in hours, or J m^{-2} if Dl is expressed in seconds.

In this equation,

$$F_b(\gamma_s, T_L(\mathrm{AM2})) = C_0 + C_1 \sin \gamma_s + C_2 \sin^2 \gamma_s \tag{20}$$

and can be re-written

$$F_b(\omega, \Phi, \delta, T_L(\mathrm{AM2})) = B_0 + B_1 \cos \omega + B_2 \cos (2\omega) \tag{21}$$

since

$$\sin\gamma_s = \sin \Phi \sin \delta + \cos \Phi \cos \delta \cos \omega. \tag{22}$$

It comes

$$B_c(\omega_1, \omega_2) = I_0 \varepsilon \left(\frac{Dl}{2\pi}\right) T_{rb}(T_L(\mathrm{AM2}))[B_0 \omega + B_1 \sin(\omega) + B_2 \sin(2\omega)]_{\omega_1}^{\omega_2} \tag{23}$$

with the coefficients B_0, B_1 and B_2 given by:

$$\begin{cases} B_0 = C_0 + C_1 \sin(\Phi)\sin(\delta) + C_2[\sin(\Phi)]^2[\sin(\delta)]^2 + 0.5\, C_2[\cos(\Phi)]^2[\cos(\delta)]^2 \\ B_1 = C_1 \cos(\Phi)\cos(\delta) + 2C_2 \sin(\Phi)\sin(\delta)\cos(\Phi)\cos(\delta) \\ B_2 = 0.25 C_2[\cos(\Phi)]^2[\cos(\delta)]^2 \end{cases} \tag{24}$$

where Φ is the latitude of the site (positive to the Northern Hemisphere) and δ is the declination (positive when the sun is north to the equator: March 21 to September 23). Maximum and minimum values of the declination are $+23°27'$ and $-23°27'$.

The B_i coefficients only depend on latitude, Φ, and declination at noon, δ. The transmission function T_{rb}, and the C_i coefficients only depend on the Linke turbidity factor for air mass 2. Thus all these factors can be computed only once for each day.

The daily integral is achieved by setting ω_1 equal to the sunrise hour angle, ω_{SR}, and ω_2 to the sunset hour angle, ω_{SS}, i.e.:

$$B_{cd} = B_c(\omega_{SR}, \omega_{SS}). \tag{25}$$

The daily sum of beam irradiation at different latitudes (30° and 60°), B_{cd}, is displayed in Fig. 6 for various turbidities, as a function of the julian day. The daily sum decreases as the turbidity increases. The distribution over the year of the daily sum is more peaked as the latitude increases, and also as the turbidity decreases.

3.2. The diffuse component

The diffuse horizontal irradiation, $D_c(\omega_1, \omega_2)$, is computed by the analytical integration of the

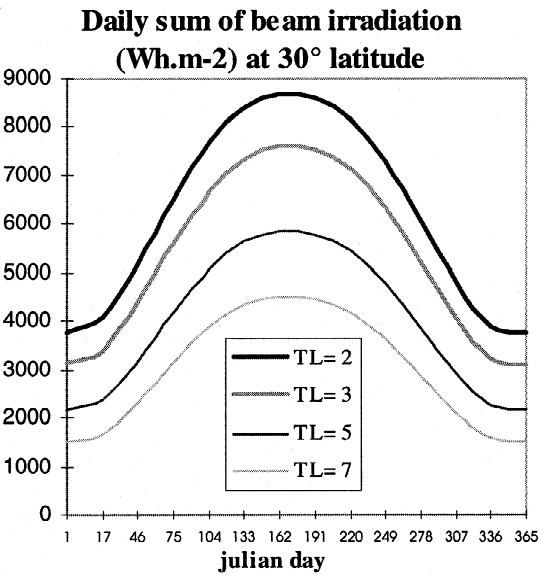

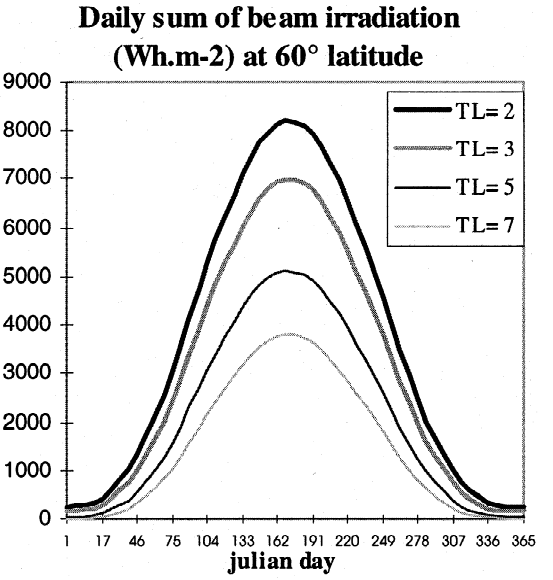

Fig. 6. The daily sum of beam horizontal irradiation for clear sky, B_{cd} computed at 30° and 60° latitude.

diffuse irradiance (Eq. (8)) over any period defined by ω_1 and ω_2, and is equal to:

$$D_c(\omega_1, \omega_2) = I_0 \varepsilon \left(\frac{Dl}{2\pi}\right) T_{rd}(T_L(\mathrm{AM2}))[D_0 \omega + D_1 \sin(\omega) + D_2 \sin(2\omega)]_{\omega_1}^{\omega_2} \tag{26}$$

with the coefficients D_0, D_1 and D_2 given by:

$$\begin{cases} D_0 = A_0 + A_1 \sin(\Phi)\sin(\delta) + A_2[\sin(\Phi)]^2[\sin(\delta)]^2 + 0.5A_2[\cos(\Phi)]^2[\cos(\delta)]^2 \\ D_1 = A_1 \cos(\Phi)\cos(\delta) + 2A_2 \sin(\Phi)\sin(\delta)\cos(\Phi)\cos(\delta) \\ D_2 = 0.25A_2[\cos(\Phi)]^2[\cos(\delta)]^2 \end{cases} \tag{27}$$

where the A_i coefficients only depend on the

Linke turbidity factor for air mass 2 and have been given previously (Eq. (11)).

The daily integral is achieved by setting ω_1 equal to the sunrise hour angle, ω_{SR}, and ω_2 to the sunset hour angle, ω_{SS}, i.e.

$$D_{cd} = D_c(\omega_{SR}, \omega_{SS}). \tag{28}$$

The daily sum of diffuse irradiation at different latitudes (30° and 60°), D_{cd}, is displayed in Fig. 7 for various turbidities, as a function of the julian day. The daily sum increases as the turbidity increases. The distribution over the year of the daily sum is more peaked as the latitude increases, and also as the turbidity increases.

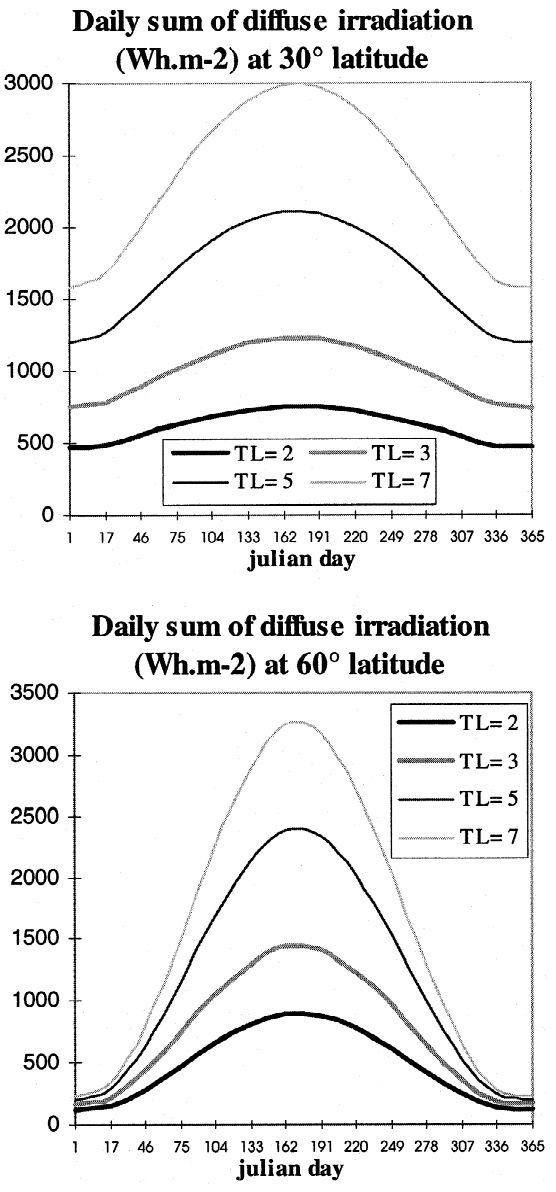

Fig. 7. The daily sum of diffuse horizontal irradiation for clear sky, D_{cd}, computed at 30° and 60° latitude.

3.3. Are both formulations equivalent?

For each component of the irradiance, two empirical formulations have been proposed in Sections 2 and 3. The first one (Section 2) has been investigated for the assessment of irradiance (W m^{-2}), and gives instantaneous values of solar radiation. The second one (Section 3) is more suitable to compute irradiation (Wh m^{-2}), since it offers an analytical function of ω, which is equivalent to the hour: thus, irradiance can be integrated analytically during the appropriate time period (for instance 1 h, or 1 day) in order to compute irradiation. To integrate irradiance, the method presented in Section 3 decomposes both the beam and the diffuse components using transmission functions and solar angular functions. Irradiation can also be computed by numerical integration of the formulation of Section 2 using fitting time steps. But, as discussed in Section 3.1, an analytical integration is easier to handle than a numerical one.

Both formulations have been compared for the computation of the clear-sky beam horizontal irradiance (Eqs. (1) and (14)). Fig. 8 displays both models for beam irradiance. The differences are small, they do not exceed 18 W m^{-2} as shown in Fig. 9 and are less than 3% for solar elevation above 25°. The diffuse irradiance has the same formulation in both sections. Therefore, the difference between the global irradiance in Section 2 and Section 3 is given by the difference between beam irradiances. Both formulations lead to very similar results and should be considered as equivalent for the assessment of the beam irradiance. Therefore, to compute the irradiation, the easiest-to-compute formulation should be preferred. The formulation of Section 3 is the simplest and should be used to compute clear-sky irradiation.

3.4. The global irradiation

The clear-sky global irradiation is obtained as the sum of the clear-sky beam horizontal irradiation and the clear-sky diffuse horizontal irradiation between two instants t_1 and t_2, according to the Eq. (19)

$$G_c(\omega_1, \omega_2) = B_c(\omega_1, \omega_2) + D_c(\omega_1, \omega_2). \tag{29}$$

The parameters ω_1 and ω_2 are respectively set to ω_{SR} and ω_{SS} for the computation of the daily sum of clear sky global irradiation:

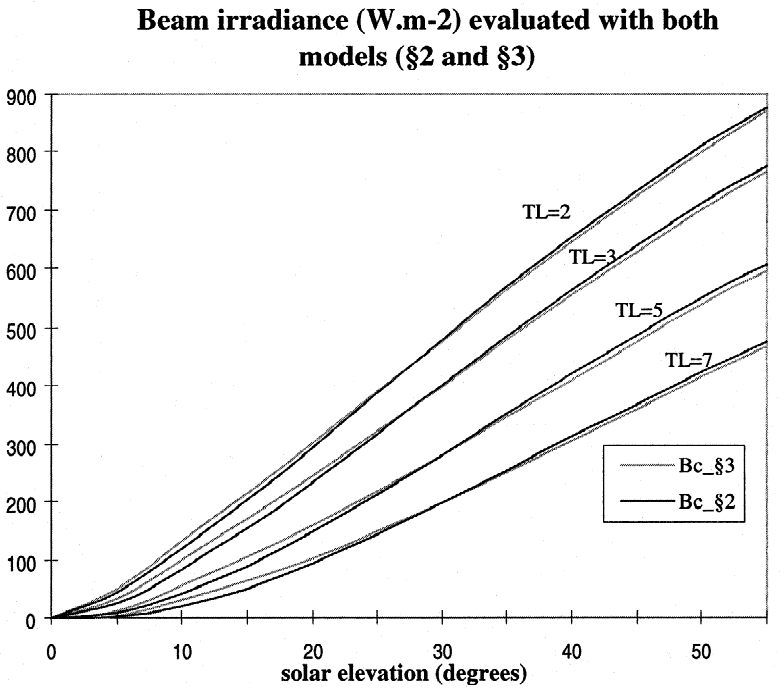

Fig. 8. Comparison between both models: Bc_§2 (Section 2) and Bc_§3 (Section 3) for the computation of the beam horizontal irradiance for clear sky. The computation has been made at mean solar distance, 45° latitude and 0° longitude (the solar declination δ is equal to 5.70°, ε is equal to 1, and $\gamma_s^{noon} > 30°$).

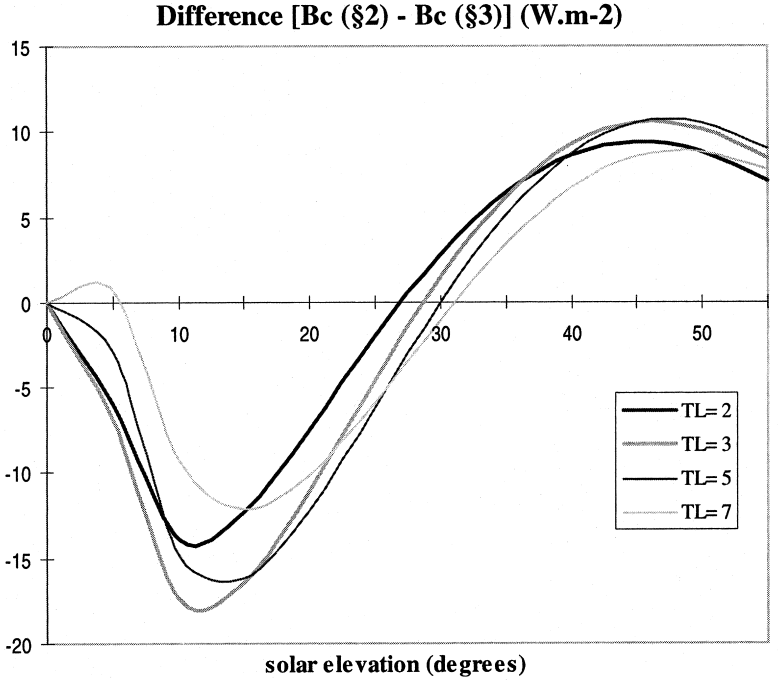

Fig. 9. Difference between Bc_§2 (beam irradiance for clear sky, Section 2) and Bc_§3 (beam irradiance for clear sky, Section 3), as a function of the solar elevation and T_L(AM2), at mean solar distance.

$$G_c(\omega_{SR}, \omega_{SS}) = B_c(\omega_{SR}, \omega_{SS}) + D_c(\omega_{SR}, \omega_{SS}) \tag{30}$$

$$\Leftrightarrow G_{cd} = B_{cd} + D_{cd}. \tag{31}$$

The daily sum of global irradiation at different latitudes (30° and 60°), G_{cd}, is displayed in Fig. 10 for various turbidities, as a function of the julian day. The daily sum decreases as the turbidity increases. The distribution over the year of the daily sum is more peaked as the latitude increases, and also as the turbidity decreases.

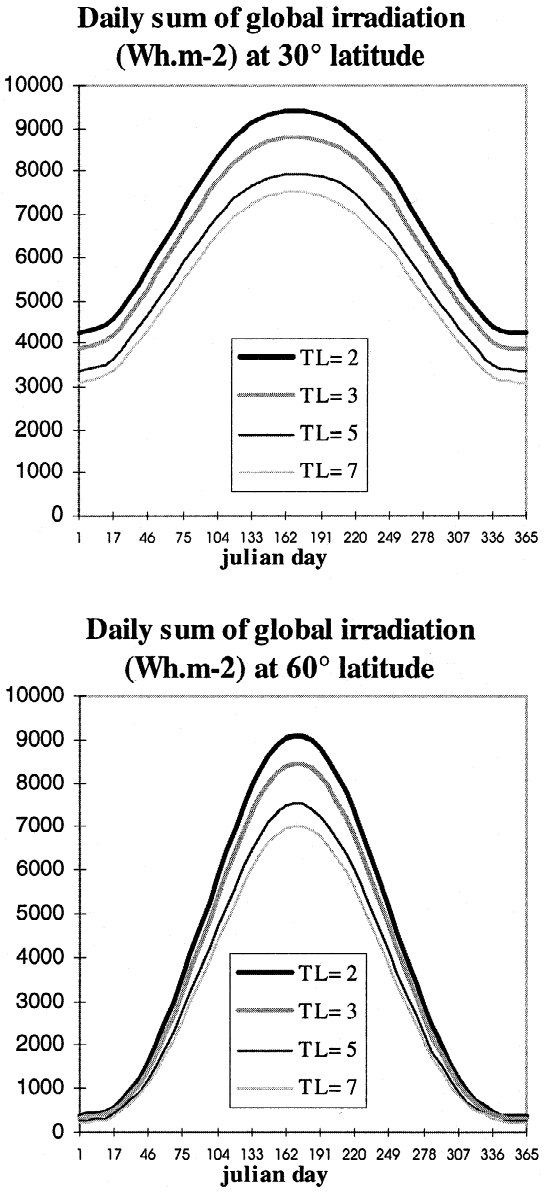

Fig. 10. The daily sum of global horizontal irradiation for clear sky, G_{cd}, computed at 30° and 60° latitude.

4. COMPARISON WITH OTHER CLEAR-SKY MODELS

4.1. Comparison with clear-sky models used previously in the Heliosat method

In the original version of the Heliosat method, Cano *et al.* (1986) used the model of Bourges (1979) to obtain the global irradiance under clear-sky:

$$G_{c(\text{Bourges})} = 0.70 I_0 \, \varepsilon \, (\sin \gamma_s)^{1.15} \tag{32}$$

Fig. 11 displays the global irradiances for this model and the ESRA model. Four different values of the Linke turbidity factor have been used: 2, 3, 5, and 7. When the solar elevation is low, both models give similar results. But when the solar elevation becomes higher than 30°, the values given by the model of Bourges are close to the values given by the ESRA model for a Linke turbidity factor between 5 and 7. Yet, in Europe, the average Linke turbidity factor is about 3.5. Therefore, the global irradiance estimated by the model of Bourges is too low for Europe, as a general rule.

The global clear-sky irradiance given by the model of Perrin de Brichambaut and Vauge (1982), hereafter noted PdBV, was used by Moussu *et al.* (1989) in their study on the Heliosat method. This model is very similar to the model of Bourges, and is given by:

$$G_{c(\text{PdBV})} = 0.81 I_0 \, \varepsilon \, (\sin \gamma_s)^{1.15} \tag{33}$$

This model, as well as that of Bourges, does not explicitly take into account the aerosols, the water content, nor the ground albedo. To check the validity of this model, Moussu *et al.* compare it to the clear-sky model described by Iqbal (1983, model C) after the works of Bird and Hulstrom (1981a,b) for various values of ground albedo, precipitable water thickness, and horizontal visibility. The comparison demonstrates that the shape of the model PdBV is consistent with the model C and that the variation of G_c is well described by the function $(\sin \gamma_s)^{0.15}$. However the magnitude of $G_{c(\text{PdBV})}$ suffers from the lack of input parameters. Fig. 11 displays also the PdBV model. One can note that for a Linke turbidity factor equal to 3, the ESRA and PdBV models give very similar values of the clear-sky global irradiance for all range of solar elevation.

Both models, $G_{c(\text{Bourges})}$ and $G_{c(\text{PdBV})}$ have been useful to establish the Heliosat method for the assessment of the solar radiation and ground

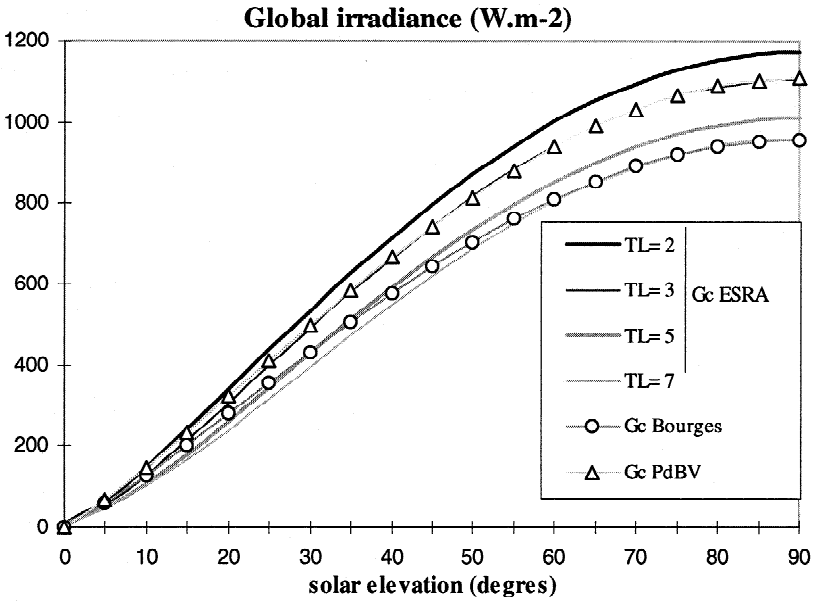

Fig. 11. Comparison between the ESRA model ($G_{c\ \mathrm{ESRA}}$) for different values of T_L(AM2), the model of Bourges, 1979 ($G_{c\ \mathrm{Bourges}}$), and the model of Perrin de Brichambaut and Vauge, 1982 ($G_{c\ \mathrm{PdBV}}$).

albedo. However their lack of accuracy prevents from further improvements in the Heliosat method. A more accurate model is needed which includes other parameters, such as the Linke turbidity factor and the elevation. A first step was made by Iehlé *et al.* (1997) who established that the introduction of the ESRA model in the Heliosat method would result in an increase of the accuracy of the estimates. They briefly examined the models of Kasten (European Solar Radiation Atlas; Palz, 1984) and of Dumortier (1995) on purely analytical grounds. They concluded that within Heliosat both models should lead to slightly larger mean bias errors than the ESRA model. Iehlé *et al.* only used one year of data for four stations in Europe. In the course of the Satellight programme funded by the European Commission (Fontoynont *et al.,* 1998), it was also concluded that the use of the Linke turbidity factor increases the accuracy of the estimates made by the Heliosat method. In this Satellight version of the Heliosat method, the clear-sky model is the one of Dumortier. Similar findings on the benefit of introducing T_L(AM2) were made by Rigollier and Wald (1999).

4.2. Comparison with other models

Other models taking into account the Linke turbidity factor and ground elevation have been compared to the ESRA model. The clear-sky irradiance given in the WMO document 557 (World Meteorological Organization, 1981, p. 124) is:

$$G_c = (1297 - 57T_L(\mathrm{AM2}))\,(\sin\gamma_s)^{[(36+T_L(\mathrm{AM2}))/33]} \tag{34}$$

Rigollier and Wald (1999) show that it provides similar results to the ESRA model. They also raise doubts on the equation for diffuse component which does not behave properly at low solar elevations (below 10–15°) and overestimates the diffuse radiation. They recommended the use of the ESRA model instead.

The model of Dumortier and a MODTRAN derived model have been retained for comparison with the ESRA model. The three models have in common the equation for beam radiation (Eq. (1)). Accordingly, the comparison is restricted to the diffuse component D_c. For validation, half-hourly measurements of either global and direct, or global and diffuse irradiation were used at seven stations for different time periods (Table 2). The diffuse, or direct component is computed by the subtraction of the measured component from the global irradiation. The instantaneous Linke turbidity factor is deduced from the measurements using Eq. (1) and assuming that the half-hourly irradiation can be assimilated to the irradiance:

$$T_L(\mathrm{AM2}) = -\ln(B_c/I_0\,\varepsilon\sin\gamma_s)/0.8662\,\delta_R(m)\,m \tag{35}$$

Table 2. Description of the ground data used to compare the diffuse clear-sky models

Station name	Latitude N; longitude E	Elevation	Available data	Period of measurement
Aas (Norway)	59.67; 10.77	85 m	Global–Diffuse	9 months (04/95–12/95)
Freiburg (Germany)	47.98; 7.83	280 m	Global–Beam	2 years (06/93–05/94 and 97–98)
Gävle (Sweden)	60.67; 17.16	16 m	Global–Diffuse	9 months (04/95–12/95)
Geneva (Switzerland)	46.20; 6.09	400 m	Global–Beam	1 year (1994, April excluded)
Oldenburg (Germany)	53.13; 8.22	20 m	Global–Beam	1 year (10/95–10/96)
Sede Boqer (Israel)	30.85; 34.78	475 m	Global–Beam	1 year (1994)
Vaulx-en-Velin (France)	45.78; 4.93	170 m	Global–Diffuse	1 year (1994)

Non clear-skies are then excluded from the measurements by excluding large values of T_L(AM2). In fact, two thresholds were used, ranging from 2.0 to 6.5, defining 15 T_L(AM2) intervals, partly overlapping each other, in order to check the influence of such choices on the conclusions: [2.0–3.5], [2.5–3.5], [3.0–3.5], [2.0–4.0], [2.5–4.0], [3.0–4.0], [2.0–5.0], [2.5–5.0], [3.0–5.0], [2.0–6.0], [2.5–6.0], [3.0–6.0], [2.0–6.5], [2.5–6.5], [3.0–6.5]. The remaining measurements were then compared to the three models of diffuse irradiance. This irradiance is also assimilated to the half-hourly irradiation for the comparison.

The model of Dumortier (1995) is defined only for solar elevation angles lower than 70°, and is given by the following expression:

$$D_c = I_0\,\varepsilon\,(0.0065 + (-0.045 + 0.0646\,T_L(\mathrm{AM2}))\sin\gamma_s - (-0.014 + 0.0327 T_L(\mathrm{AM2}))\sin^2\gamma_s) \quad (36)$$

with the conditions: $\gamma_s < 70°$ and $2.5 \leq T_L(\mathrm{AM2}) \leq 6.5$.

The third model was developed at the University of Oldenburg (Beyer *et al.,* 1997) using the radiative transfer code MODTRAN 3.5 (Kneizys *et al.,* 1996). Various simulations were made using various sets of parameters. The following expression was found to fit well the outputs of MODTRAN:

$$D_c = I_0\,\varepsilon(a + bT_L(\mathrm{AM2}) + cT_L(\mathrm{AM2})^2 + (d + eT_L(\mathrm{AM2}) + fT_L(\mathrm{AM2})^2)\sin\gamma_s + (g + hT_L(\mathrm{AM2}) + iT_L(\mathrm{AM2})^2)\sin^2\gamma_s) \quad (37)$$

$a = 0.017991$ $d = -0.112593$ $g = -0.019104$
$b = -0.003967$ $e = 0.101826$ $h = -0.022103$
$c = 0.000203$ $f = -0.006220$ $i = 0.003107$

Fig. 12 displays these three models for a Linke turbidity factor of 3 and 6. These models are quite similar for low solar elevation and diverge at high elevation.

For each remaining measurement, the three models were performed using the corresponding half-hourly T_L(AM2) value. The differences between the model estimates and the observations were computed and then summarised as bias

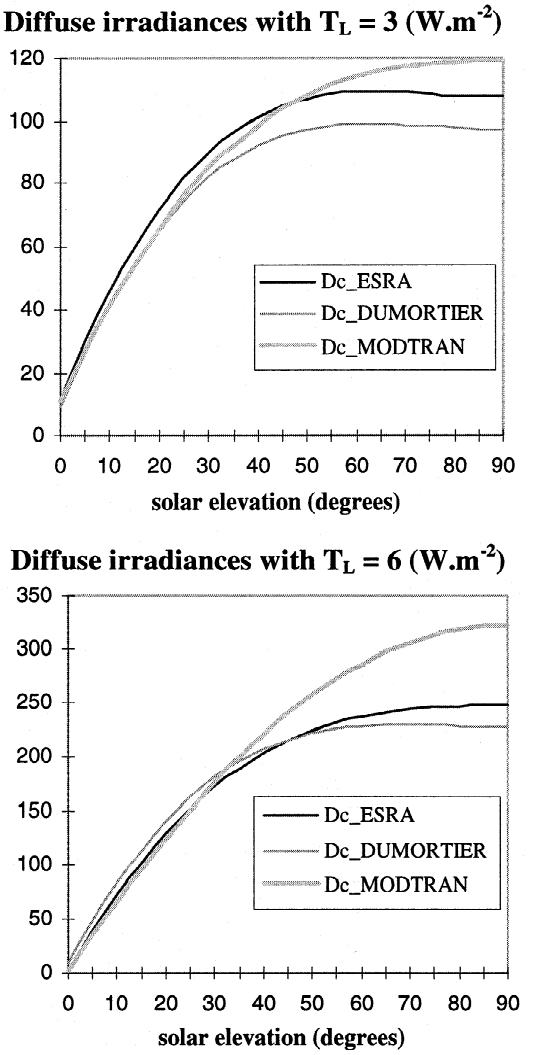

Fig. 12. The diffuse components of the ESRA model ($D_{c\ \mathrm{ESRA}}$), the Dumortier model ($D_{c\ \mathrm{Dumortier}}$), and the MODTRAN model ($D_{c\ \mathrm{MODTRAN}}$) for T_L(AM2)=3 and 6, at mean sun–earth distance.

Table 3. Results in Wh m^{-2} obtained when comparing the diffuse models of Dumortier, ESRA, and MODTRAN with half-hourly values. Only the values corresponding to a T_L(AM2) between 2.5 and 6.5 have been retained. All values of solar elevations are kept

	Ground	ESRA		Dumortier		MODTRAN	
	mean	Rmse	Bias	Rmse	Bias	Rmse	Bias
Aas	85	23 (27%)	1	23 (27%)	−1	22 (26%)	1
Freiburg 93	135	33 (24%)	−14	35 (26%)	−17	28 (21%)	−7
Freiburg 97	99	30 (30%)	13	29 (29%)	10	35 (35%)	17
Gävle	111	27 (24%)	−10	29 (26%)	−14	26 (24%)	−10
Geneva	103	33 (32%)	14	31 (30%)	10	40 (39%)	19
Oldenburg	105	26 (25%)	−5	27 (25%)	−7	26 (25%)	−4
Sede Boqer	102	26 (26%)	10	24 (24%)	5	27 (27%)	15
Vaulx-en-Velin	112	27 (24%)	6	27 (24%)	4	33 (30%)	13

(estimates mean minus observations mean) and root mean square error (rmse) for each range of T_L(AM2) and some ranges of solar elevation (Table 3).

When comparing the different models, the results obtained show that the three clear-sky models give similar results. None of the models always give the best results. However, one can note that the ESRA clear-sky model never gives the worst errors. Therefore it may be considered as the most robust of the three models. This property is a key point when automatic processing of large volumes of data is at stake. For this reason, the ESRA clear-sky model should be preferred. For this model, the rmse is comprised between 11 and 35 Wh m^{-2}, for all ranges of T_L(AM2) for diffuse irradiation up to 250 Wh m^{-2}. There is no significant dependence of the results on the geographical location and on the ground elevation. The results obtained for Freiburg, where two datasets of 1 year are available, show a high temporal variability.

We have validated these conclusions with another dataset of seven stations which is more expanded in time: from 1981 to 1990, but it offers a lower geographical coverage (Table 4). This dataset is extracted from the ESRA. Uccle offers half-hourly measurements of global, diffuse and beam irradiations, while only hourly sums of global and diffuse irradiation are available for the other stations.

The results computed over 10 years show that even if the errors are similar for the three models, the ESRA model always gives the best results for all stations when considering average errors over the 10 years. In Tables 5 and 6 are reported root mean square errors (rmse) and bias for the three models, and for two ranges of T_L(AM2).

The results are slightly the same for the different sites. There is still no significant dependence of the results on ground elevation or geographical location. Moreover, the differences in error observed in 1994 between two remote sites such as Sede Boqer and Vaulx-en-Velin are not higher

Table 4. Description of the second dataset of ground stations. The data are measured from January 1981 to December 1990

Station name	Latitude N; longitude E	Elevation	Station name	Latitude N; longitude E	Elevation
Braunschweig (Germany)	52.30; 10.45	83 m	Würzburg (Germany)	49.77; 9.97	275 m
Dresden (Germany)	51.12; 13.68	246 m	Weihenstephan (Germany)	48.40; 11.70	472 m
Hamburg (Germany)	53.65; 10.12	49 m	Uccle (Belgium)	50.80; 4.35	100 m
Trier (Germany)	49.75; 6.67	278 m			

Table 5. Results in Wh m^{-2} obtained when comparing the diffuse models of ESRA, Dumortier, and MODTRAN with hourly values of the second ground dataset. T_L(AM2) ranges from 2.5 and 3.5

	Ground	ESRA		Dumortier		MODTRAN	
	mean	Rmse	Bias	Rmse	Bias	Rmse	Bias
Braunschweig	79	19 (24%)	−8	22 (28%)	−15	22 (28%)	−11
Dresden	61	13 (22%)	−2	15 (25%)	−8	16 (26%)	−6
Hamburg	70	15 (22%)	−3	18 (25%)	−9	18 (25%)	−6
Trier	76	17 (22%)	−3	19 (25%)	−10	19 (25%)	−6
Würzburg	76	17 (23%)	−5	20 (27%)	−12	20 (26%)	−9
Weihenstephan	72	20 (27%)	−1	21 (29%)	−7	21 (30%)	−4
Uccle	66	16 (25%)	−1	17 (26%)	−7	18 (27%)	−4
All stations	71	17 (24%)	−3	19 (27%)	−9	19 (27%)	−7

Table 6. As Table 5 but for T_L(AM2) ranging from 2.5 to 6.5

	Ground	ESRA		Dumortier		MODTRAN	
	mean	Rmse	Bias	Rmse	Bias	Rmse	Bias
Braunschweig	121	23 (19%)	−10	25 (21%)	−11	23 (19%)	−7
Dresden	101	19 (19%)	1	20 (20%)	0	22 (22%)	3
Hamburg	107	20 (19%)	−5	21 (20%)	−6	21 (20%)	−4
Trier	119	23 (19%)	−7	25 (21%)	−10	23 (19%)	−4
Würzburg	120	22 (19%)	−7	24 (20%)	−9	23 (19%)	−4
Weihenstephan	114	24 (21%)	−2	25 (22%)	−4	26 (23%)	2
Uccle	110	20 (18%)	−2	21 (19%)	−4	21 (19%)	0
All stations	113	22 (19%)	−5	23 (21%)	−6	23 (20%)	−2

than those observed between 1981 and 1990 for the different German stations. This low spatial variability allows to conclude that the model is not affected by the climate. The high temporal variability noted for Freiburg between results in 1993 or in 1997 is also observed for this 10-year dataset. For example, for a Linke turbidity factor ranging from 2 to 3.5, rmse of the ESRA model are varying from 11 to 18 Wh m^{-2} in Hamburg while the 10-year error is 15 Wh m^{-2}. In Weihenstephan, rmse are varying from 14 to 25 Wh m^{-2} while the 10-year error is 19 Wh m^{-2}. Half-hourly values are available for Uccle, therefore a computation has been made to get hourly values in order to compare errors obtained from these two kinds of data. Similar numbers are observed for the assessment of the irradiation on an hourly basis than those obtained from half-hourly basis.

Tables 7 and 8 report values of rmse, relative rmse, and bias for the ESRA model and selected solar elevations: $20° \leq \gamma_s \leq 25°$, $40° \leq \gamma_s \leq 45°$, and $60° \leq \gamma_s \leq 65°$. These tables have been drawn for Würzburg, but are representative of the other German stations since there is no climate effect. On the one hand, there is no clear dependence on the solar elevation within the results, even if the errors are varying from one range to another. On the other hand, these tables illustrate the importance of the selection of the range of T_L(AM2) on the results. The rmse in Wh m^{-2} decreases when skies are getting clearer. This holds for all models and all ranges of solar elevation and numbers should be considered with care. However the conclusions drawn are valid for all ranges of T_L(AM2).

In this study, Eq. (1) was used to compute T_L(AM2) for the sake of the simplicity. If the second formulation (Eq. (14)) had been used, it would have resulted in slightly different T_L(AM2) values but similar errors than the first formulation.

5. CONCLUSION

We have analysed the models proposed by the new digital European Solar Radiation Atlas (ESRA) for the assessment of the irradiance and the irradiation under clear sky for both the beam and the diffuse components. We have investigated the variations of these models with various parameters, namely the sun elevation and the Linke turbidity factor. The ESRA proposes two sets of models. One is best suited for the assessment of the irradiance. The other should be preferred for the computation of hourly irradiation and daily sum of irradiation. We conclude that these models can be used in the framework of the Heliosat method, especially the second one, since the aim of the Heliosat method is to estimate solar irradiation received at ground level from satellite images.

Table 7. Results in Wh m^{-2} obtained for different ranges of solar elevation when comparing the diffuse ESRA model with hourly values measured in Würzburg (Germany). Only the values corresponding to a Linke turbidity factor between 2.5 and 6.5 have been retained

Solar elevation	Number of values	Ground mean	Bias	Rmse	Relative rmse
60°–65°	243	197	−16	32	16%
40°–45°	717	174	−11	27	16%
20°–25°	1236	118	−7	22	18%

Table 8. As Table 7 but with T_L(AM2) ranging between 2.5 and 3.5

Solar elevation	Number of values	Ground mean	Bias	Rmse	Relative rmse
60°–65°	29	109	5	21	19%
40°–45°	73	105	1	19	18%
20°–25°	235	86	−7	20	23%

The ESRA model has been compared to several other clear-sky models and has proved to be the most accurate as a whole, though other models lead to similar results.

Compared to the other models used up to now in the Heliosat method, the accuracy in the ESRA model is mostly gained by the introduction of the Linke turbidity factor. From an operational point of view, the use of the ESRA model implies the knowledge at each pixel of the image, of the Linke turbidity factor and of the ground elevation. Digital maps of ground elevation are currently available for the whole Earth with a spatial resolution suitable for the processing of images from the meteorological satellites. Accuracy elevation may be questioned in several parts of such maps. However the impact of this accuracy on the outputs of the ESRA model is less than the impact of an error on T_L(AM2). This factor is hardly known everywhere and an effort should be devoted to its assessment at each pixel of the image, at least on a climatological basis, season by season.

These models have been coded in language C and should be available as sources at the WWW site Helioserve: www-helioserve.cma.fr/. In this site, the user can already simulate the clear-sky irradiation, given the geographical site, the elevation and the Linke turbidity factor. A database of the Linke turbidity factor has also been set up for about 500 sites. These values are available in this WWW site and can be used for a better assessment of the clear-sky radiation (Angles *et al*., 1998).

Acknowledgements—The content of the present paper was influenced by some chapters of the ESRA handbook. Fruitful discussions with John Page (Sheffield, UK) have helped to improve the clearness of this article. The authors deeply acknowledge the help of the University of Oldenburg (Germany); part of this work was done there using their valuable softwares and databases. This work was partly supported by the programme JOULE of the European Commission (DGXII): programmes ESRA (co-ordinator: K. Scharmer, GET, Germany) and SatelLight (co-ordinator: M. Fontoynont, ENTPE, France).

REFERENCES

Angles J., Menard L., Bauer O. and Wald L. (1998) A Web server for accessing a database on solar radiation parameters. In Proceedings of the Earth Observation and Geospatial Web and Internet Workshop '98, Vol. Heft 27, Strobl J. and Best C. (Eds.), pp. 33–34, Salzburger Geographische Materialien, Universität Salzburg, Salzburg, Austria.

Beyer H. G., Hammer A., Heinemann D. and Westerhellweg A. (1997) Estimation of diffuse radiation from Meteosat data. In *North Sun '97, 7th International Conference On Solar Energy at High Latitudes, Espoo-Otaniemi, Finland.*

Bird R. and Hulstrom R. L. (1981a) Direct insolation models. *Trans. ASME J. Solar Energy Eng.* **103**, 182–192.

Bird R. and Hulstrom R. L. (1981b). *A simplified clear sky model for direct and diffuse insolation on horizontal surfaces. Report SERI/TR-642-761,* Solar Energy Research Institute, Golden, CO, USA.

Bourges G. (1979) Reconstitution des courbes de fréquence cumulées de l'irradiation solaire globale horaire reçue par une surface plane. In Report CEE 295-77-ESF, Vol. tome II, Centre d'Energétique de l'Ecole Nationale Supérieure des Mines de Paris, Paris, France.

Cano D., Monget J. M., Albuisson M., Guillard H., Regas N. and Wald L. (1986) A method for the determination of the global solar radiation from meteorological satellite data. *Solar Energy* **37**, 31–39.

Dumortier D. (1995) Modelling global and diffuse horizontal irradiances under cloudless skies with different turbidities. In *Final Report JOU2-CT92-0144, Daylight II*, Ecole Nationale des Travaux Publics de l'État, Vaulx-en-Velin, France.

Fontoynont M., Dumortier D., Heinemann D., Hammer A., Olseth J., Skartveit A., Ineichen P., Reise C., Page J., Roche L., Beyer H. -G. and Wald L. (1998) Satellight: a WWW server which provides high quality daylight and solar radiation data for Western and Central Europe. In Proceedings of the 9th Conference On Satellite Meteorology and Oceanography, Vol. EUM P 22, pp. 434–435, Eumetsat, Darmstadt, Germany.

Iehlé A., Lefèvre M., Bauer O., Martolini M. and Wald L. (1997). In *Meteosat: a valuable tool for agro-meteorology*, Joint Research Center, Ispra, Italy, Final Report for the European Commission.

Iqbal M. (1983). In *An Introduction To Solar Radiation*, pp. 107–169, Academic Press, New York.

Kasten F. and Young A. T. (1989) Revised optical air mass tables and approximation formula. *Appl. Opt.* **28**(22), 4735–4738.

Kasten F. (1996) The Linke turbidity factor based on improved values of the integral Rayleigh optical thickness. *Solar Energy* **56**, 239–244.

Kneizys F. X. et al. (1996). In *The MODTRAN 2/3 Report and LOWTRAN 7 Model. Technical Report*, Phillips Laboratory, Geophysics Directorate, Hanscom AFB.

Moussu G., Diabate L., Obrecht D. and Wald L. (1989) A method for the mapping of the apparent ground brightness using visible images from geostationary satellites. *Int. J. Remote Sensing* **10**(7), 1207–1225.

Page J. K. (1995). *The estimation of diffuse and beam irradiance, and diffuse and beam illuminance from daily global irradiation, a key process in the evolution of microcomputer packages for the new European Solar Radiation and Daylighting Atlases*, Technical Report No. 8, prepared June 30th, 1995 and revised August 6th, 1995, 37+5 pp. of tables. Appendix 1: Solar elevation functions for estimating cloudless day beam irradiance and daily beam irradiation on horizontal surfaces from the beam transmittance, 12 pp.+5 pp. of tables. Page, J.K., 1996. Technical Report No. 8, revised September 21st, 1996, 36 pp.+5 pp. of tables. Appendix 1: Revised September 22nd, 1996, 13 pp.+5 pp. of tables.

Perrin de Brichambaut C. and Vauge C. (1982). *Le gisement solaire: evaluation de la ressource énergétique,* Technique et documentation (Lavoisier), Paris.

Rigollier C. and Wald L. (1999) Selecting a clear-sky model to accurately map solar radiation from satellite images. In *Proceedings of the 19th EARSeL Symposium 'Remote Sensing in the 21st Century: Economic and Environmental Applications', Valladolid, Spain*, Nieuwenhuis G., Vaughan R. and Molenaar M. (Eds.), Balkema.

Second Improved and Extended Edition, (1984). European Solar Radiation Atlas, vols. I and II, Palz W. (Ed.), Commission of the European Communities, DG Science, Research and Development, Bruxelles, Report No. EUR 9344.

Wald L., Albuisson M., Czeplak G., Bourges B., Aguiar R., Lund H., Joukoff A., Terzenbach U., Beyer H. G. and Borisenko E. P. (1999). In 4th ed including CD-ROM, ESRA — European Solar Radiation Atlas, Greif J. and Scharmer K. (Eds.), Commission of the European Communities by Presses de l'Ecole, Ecole des Mines de Paris, Paris, France, Scientific advisors: R. Dogniaux, J.K. Page.

World Meteorological Organization (1981). In *Meteorological Aspects of the Utilization of Solar Radiation as an Energy Source. Annex: World Maps of Relative Global Radiation. Technical Note No. 172, WMO-No. 557*, p. 298, WMO, Geneva, Switzerland.